Journal of Constructional Steel Research 143 (2018) 162–179

Contents lists available at ScienceDirect

Journal of Constructional Steel Research

Thermal buckling behaviour of unstiffened and stiffened fixed-roof tanks under non-uniform heating

Daphne Pantousa *, Konstantinos Tzaros, Maria-Alexandra Kefaki

Laboratory of structural analysis and design, Department of Civil Engineering, University of Thessaly, Pedion Areos, Volos, Greece

ARTICLE INFO

Article history:
Received 2 September 2017
Received in revised form 12 December 2017
Accepted 17 December 2017
Available online xxxx

Keywords:
Thin-walled tanks
Fire
Non-uniform heating
Buckling
Numerical analysis

ABSTRACT

The problem addressed in this paper is the thermal buckling behaviour of thin-walled steel cylindrical fixed-roof tanks under non-uniform loading, induced by an adjacent tank. This specific type of thermal loading can be triggered by a neighboring tank fire where heat is transferred mainly through radiation. Since the calculation of the temperature field of the heated tank lies in other scientific fields (e.g. Computational Fluid Dynamics), a thermal pattern, proposed in literature, is used for the simulation of the fire-induced load and the investigation of the structural response of the tank due to heating. The study is conducted numerically through the Finite Element method, using coupled thermo-mechanical analysis. The general purpose Finite Element code MSC Marc, is used for the simulation. Three-dimensional models are developed using shell elements. Firstly, a detailed study of the failure mechanisms that take place in case of non-uniform loading is carried out. Furthermore, tanks with different geometries are studied. The main objective is the calculation of the critical temperature i.e. the temperature where the failure appears and the determination of the failure modes. Finally, a parametric study is conducted for the evaluation of the effectiveness of stiffening methods that are commonly used at ambient temperature design (stiffeners and stepwise wall thickness), in the case of the non-uniform heating load. In this study, the heated tanks are considered to be empty, which is the most severe scenario, for their structural integrity.

1. Introduction

Tank fire incidents take place mainly in petroleum refineries, oil terminals or storage tank facilities and they can be catastrophic. Current regulations (API 650 [1], NFPA 30:2012 [2]) define strict guidelines for construction, material selection, design and safe management of storage tanks and propose active fire protection measures in order to minimize the risk of fire and to prevent fire spreading. Nevertheless, the structural design of storage tanks under thermal loading is not covered by the existing guidelines.

Although most companies strictly follow the regulations, tank fire accidents still occur. According to [3], in total 480 tank fire incidents have been identified worldwide from 1950 until 2003 and the number of incidents increases each decade. International attention was given to the tank fire event that took place in 2005 at the Buncefield Oil Storage Depot in the north of London. This event motivated scientific research in order to better understand the major cause of tank explosions and spreading of fires. Moreover, recently (2015), a massive fire and explosion of oil tanks in a storage facility near Kiev resulted in serious environmental impact.

Storage tanks that are used for liquid hydrocarbons (e.g. oil, diesel etc.), are classified according to the operation pressure and the type of roof that is used. Specifically, the atmospheric tanks can be designed as open or with roofs which can be either floating or fixed. Floating roof tanks are used for storage of liquid hydrocarbons which are characterized by a low ignition point (lower than standard ambient temperature) like light crude oil and light polar compounds (methanol, ethanol, ketones etc.). Fixed-roof tanks are used for heavy oil products (like diesel and mazut) with an ignition point greater than ambient temperature. According to the literature, the floating roof tanks minimize losses and escape of volatiles to the environment and they are considered the safest storage facilities for oil products. Fixed-roof tanks with cone roofs is the most common type of tanks that is used in practice and this study is focused on these types of tanks.

Tank fire incidents may be initiated due to several reasons like operating errors, equipment failure, lightning, poor maintenance, static electricity and so on. Moreover, a domino chain can be triggered in case of earthquake, as e.g. it was reported after the Izmit earthquake of 1999 in Turkey [4]. The fire may be limited to one tank but there is a serious possibility that the fire will spread to the adjacent tanks due to fuel leakage or due to thermal radiation. In case of a fire in a fixed-roof tank that contains flammable liquid, it is possible that the volatiles in the vapor space above the liquid in the interior of the tank, will ignite

* Corresponding author at: Pedion Areos, Volos, Greece.
E-mail address: dpantousa@uth.gr (D. Pantousa).

https://doi.org/10.1016/j.jcsr.2017.12.018
0143-974X/

if the right conditions appear. The ignition may result to structural failure as it is possible that the roof will partially detach from the cylindrical wall of the tank (failure known as large 'cod's mouth' rupture) leaving the tank wall and its contents exposed. Under these circumstances a full surface fire will be initiated. In this case, the fire is very difficult to be suppressed and the phenomenon will continue until the total volume of the flammable liquid is consumed. The duration of such fires varies between one and three days depending on the available volume of the stored liquid. If the fire will not spread to the neighboring tanks, the burning tank constitutes a heat generator for the adjacent tanks. The heat is transferred mainly through radiation and generates thermal loading.

Nowadays, the interest of the researchers is focused on the prediction of heat transfer characteristics of pool fires ([5,6,7,8]), their effect (radiation, temperature field etc.) on adjacent "target" tanks ([9]), the thermal response of stored liquid in adjacent tanks ([6]) and the potential of escalating fire involving more tanks ([10,11]). Most of the published studies agree that the safety distances between the tanks proposed in the current regulations should be reconsidered. Specifically, in the study of Silva Santos and Landesmann [11] it is indicated that the minimum safety distances change rapidly due to the wind and that the present NFPA30:2012 recommendations need to be modified, in order to achieve a satisfactory failure prediction for different storage fuels (e.g. ethanol).

The thermal buckling of cylindrical shells was studied in the past for uniform heating and temperature gradients ([12,13,14,15,16,17]). But the thermal loading generated by fire is more complicated than the patterns studied previously. According to Godoy [18] the research concerning the structural performance of thin-walled steel tanks has recently been started and is limited ([19,20,21,22]). The doctoral thesis of Liu [19] was the first and most complete study in this area and presents a systematic exploration of the potential thermal and structural behaviour of an oil tank when one of its neighboring tanks is on fire. One of main objectives of this thesis was to reveal the thermal distribution patterns developed in an oil tank under the heating from an adjacent tank fire. The study proposes a simplified temperature distribution that follows a cosine function along the circumferential coordinate, while in the vertical direction the distribution is uniform. Moreover, the thesis reveals the underlying mechanisms responsible for the buckling of tank structures and examines the influences of various thermal and geometrical parameters on the buckling temperature of the tanks.

The papers of Godoy and Batista ([20,21]) adopt this thermal pattern, proposed in Liu's thesis [19], and study the structural behaviour of fixed-roof and open tanks heated by an adjacent fire-engulfed tank. Specifically, in [20], two tanks that buckled under a huge fire in Bayamon, Puerto Rico in 2009, are investigated in detail. Parametric studies are performed to understand the influence of the shell thickness, the level of fluid stored in the tank, the area affected by fire in the circumferential direction and the temperature gradient through the thickness. The open cylindrical storage tanks are studied in [21]. The results for open tanks show that the location of large out-of-plane displacements attributable to thermal buckling coincides with the heated zone. The importance of thermal gradients in the thickness of the tank walls to the buckling load and mode are shown.

According to the findings of the aforementioned studies, the temperature field of a tank that is heated by an adjacent tank, is non-uniform in both vertical and circumferential directions and depends on several factors such as the distance between them, the diameter of both the burning and the heated tank, the type of burning liquid, the speed and the direction of the wind and so on. Thus, there exists an important temperature difference between the hotter and the colder part of the heated tank and significant compressive stresses may arise due to restrained thermal expansion. The reduction of mechanical properties of steel in conjunction with the thermal induced stresses may lead to thermal buckling and failure of the tank in relatively low temperatures.

The basic objective of this paper is to study thoroughly the behaviour of thin-walled steel tanks with fixed roof under non-uniform heating that is generated from an adjacent fire-engulfed tank. Specifically, first a detailed research is conducted in order to understand the failure mechanisms of tanks during non-uniform heating. Then, thin-walled tanks with different slenderness (height to diameter ratio) that are commonly used in practice are studied, in order to reveal the effect of several parameters (initial imperfections, boundary conditions etc.) in the response of heated tanks and to investigate the effectiveness of the strengthening methods that are commonly used at ambient temperature design (stiffeners and stepwise wall thickness) in the case of non-uniform heating load. The heated tanks are considered to be empty, which is the most severe scenario, according to the findings of literature. The problem is solved numerically through the Finite Element method.

2. Description of the problem - the case studies

The problem considered in this paper is the study of the behaviour of a heated fixed-roof tank when the thermal loading is generated from a fire-engulfed adjacent tank and the dominant mechanism of heat transfer is radiation. In the case where the thermal loading, it is expected that the temperature distribution of the heated tank will be non-uniform. Actually, the study lies on the scientific area of the behaviour of thin-walled shells. As it is well known, these shells are commonly used in many applications of engineering sustaining the loading mainly through the membrane actions. Even though, they are very efficient, they are vulnerable to buckling failure due to the compressive forces that may appear. In this case, important displacements arise and the membrane energy is transformed to bending energy. This type of failure can be induced by mechanical or thermal loading. The present study investigates the thermal buckling of thin-walled cylindrical shells for non-uniform thermal loading.

Specifically, the side of the tank which is facing the source tank (which is on fire) is hot, compared to the opposite face which is not affected by the fire. The higher temperature of the heated tank is detected at the meridian of the tank which is closest to the fire and the temperature decreases at the meridians that are further away along the circumference. Moreover, it is logical to assume that the level of the stored liquid can affect the temperature pattern in the vertical direction. In particular, the upper part of the tank which is not in contact with the stored liquid is heated more than the lower part, due to the fact that the heat transfer coefficient of air is low (in the upper part) and the thermal inertia of the stored liquid is high (in the lower part). As it is indicated in other studies, the tank is more vulnerable when it is empty, since the stored liquid (due to the high thermal inertia) affects the temperature of the walls of the tank and prevents the stability phenomena that may lead to failure. Thus, this paper studies only the case of empty tanks.

The phenomenon is complicated and it is difficult to predict the temperature distribution of the heated tank. Pool-fire semi-empirical models, available in the literature, can be used to determine the characteristics of flames generated at the fire-tank. Then, the temperature distribution of the heated tank walls can be found numerically through Computational Fluid Dynamics analysis or through the Finite Element method. Since the evaluation of the temperature field of the heated tank lies on another scientific area, it is out of the scope of this paper. Liu [18] conducted a detailed numerical study and the results are found to be reasonable and describe adequately the complicated phenomenon. This study adopts the simplified model proposed in [18]. The temperature distribution of the heated tank is described by the pattern of Fig. 1 and Eq. (1). In this study it is assumed that the source tank is of the same diameter as the target tank and that the distance between them has also the same magnitude. In this

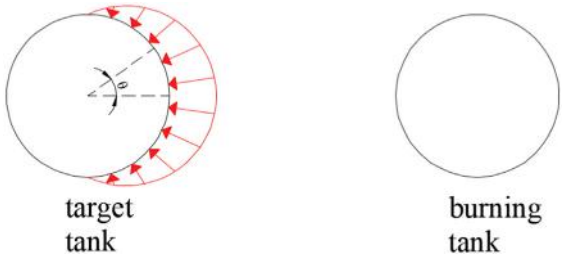

Fig. 1. Temperature pattern of the heated tank and the equation that describes the pattern.

case only half of the heated tank is submitted to a rise in temperature.

$$T_\theta = \begin{cases} (T_{0m} - T_{0a}) \cos^2\left(\frac{\theta}{\theta_0}\right) & if \ |\theta| \le \theta_0 \\ 0 & if \ |\theta| > \theta_0 \end{cases} \quad (1)$$

In Eq. (1), θ is the circumferential coordinate, θ_0 is the critical angle that defines the heated zone, T_{0m} is the temperature of the most heated meridian and T_{0a} is the ambient temperature. In the vertical direction, the temperature is considered to be constant.

This paper studies four different thin-walled steel fixed-roof tanks with cylindrical bodies which are used for the storage of flammable liquids like diesel and mazut. For a diameter equal to 20 m, three different cases are examined with a height equal to 10 m, 20 m and 40 m respectively. Additionally, a tank of 40 m in diameter and 20 m high is studied. Table 1 presents the geometric characteristics of the tanks and the notation that is used in the following. First the study is focused on the reference case of the tank a diameter and height equal to 20 m in order to investigate in detail the behaviour of the cylindrical tank under non-uniform heating and to validate the numerical model against published results available in previous steadies. Next, the other tanks are examined and the results reveal the effect of the slenderness of the tanks on their behaviour.

In all cases, the roof is considered to be a conical shell with a slope equal to 10° (when it is measured with respect to the horizontal line). In practice, the type of roof that is used depends mainly on the diameter of the cylindrical tank and as the diameter increases it is more realistic to choose internal trusses to support the roof. Nevertheless, in this study the roof is simulated as a conical shell in order to simplify the calculations. According to findings of Liu [19], the buckling may appear first either to the roof or to the cylindrical shell. The first case is likely to happen but this paper is focused on the phenomena that take place in the tank walls. The study of the roof's failure would require the realistic simulation of its static system. A recent study of Burgos [22], considers the structural consequences of such simplifications, including the substitution of a supporting structure of the roof, in detail. Here, the roof is included in the numerical model, aiming only to simulate the boundary conditions at the top of the cylindrical shell in a realistic way. Moreover, the induced restraint depends on the stiffness of the roof which is determined by the type of static system (e.g. beams, trusses etc.) and the constructed end conditions. The latter provides a certain restraint at the top of the shell, which, in order to simplify the numerical model, can be represented by only one parameter, i.e. the thickness of the roof shell. Therefore, parametric studies are conducted

Table 1
The case studies.

	Tank A	Tank B	Tank C	Tank D
Diameter (m)	20	20	20	40
Height (m)	20	10	40	20

Table 2
Variation of roof's self – weight with the diameter.

Diameter	10	20	40
Self - weight of roof (kg)/m^2	20	40	80

in order to discover the effect that the stiffness of the roof has onto the behaviour of the heated tank. Roof stiffness is modified using different magnitudes of shell thickness (i.e. an *equivalent* thickness) and two extreme cases are considered. The smaller value of the *equivalent* thickness of the roof shell (t_r) is taken equal to five times the thickness of the cylindrical tank (t_c) and on the other side it is considered sixty times thicker. A parametric study is performed for intermediate values i.e. $5t_c \le t_r \le 60t_c$.

3. Numerical modeling

The problem is solved numerically using the Finite Element (FE) method. Other different numerical methods such as the Boundary Element Method [23] and Isogeometric analysis [24,25] can also be employed for the prediction of the buckling behaviour of the cylindrical shell tanks. In this study, the numerical model is developed using the nonlinear finite element code MSC-Marc [26]. The three-dimensional model that is developed for the simulation of the behaviour of the thin-walled steel tank uses the element 75 of the program's library, which is actually one of the most robust shell elements, because eliminates the locking phenomenon when it is used for thin shell applications. Element 75 is a four-node, Mindlin type, thick-shell element with six degrees of freedom in each node, i.e. three translational in the global directions x, y,z, and three rotational degrees of freedom about global x, y, z-axis respectively. The shape functions of the element are bilinear thus, bilinear interpolation is used for the description of the geometry and the displacement and rotation fields inside the element. Then, based on the constitutive law and the kinematic conditions the membrane strains are obtained from the displacement field, while the curvatures from the rotation field. All the types of nonlinearity can be considered with the certain element. Regarding the evaluation of the stiffness matrix of the element, the Gauss method is considered and the numerical integration is implemented through the utilization of four Gauss points (Full Integration). However, the theoretical formulation of the specific thick shell element has been developed so that there is no locking when it is used for thin shell applications [26]. It is noted that the problem of locking can be treated successfully using techniques proposed in literature, e.g [27,28,29,30]. In the specific element used in this study, a special formulation is used, where the transverse shear strains are calculated at the middle of the edges and interpolated to the integration points, according to [31,32,33]. Shear interpolations are then created throughout the element from these points in an indirect way. Through this formulation, the element retains the proper rank and, hence, cannot exhibit various kinds of spurious behaviour. The material properties are temperature dependent as it is proposed in EN 1993-1-2.

Table 3
Results of mesh sensitivity study.

	Circumferential mesh	Vertical mesh (coarse zone)	Vertical mesh (fine zone)	Critical temperature
1	0.5°	0.025m	0.1m	108.45°C
2	0.5°	0.025m	0.25m	108.6°C
3	1°	0.05m	0.5m	110°C
4	1°	0.025m	0.25m	120.5 °C
5	1°	0.05m	0.5m	122°C
6	3°	0.025m	0.25m	164°C
7	3°	0.05m	0.5m	167°C
8	6°	0.025m	0.25m	195°C
9	6°	0.05m	0.5m	197°C

Table 4
Buckling temperature (in °C) for all case studies for different roof to cylindrical shell thickness ratios.

Tank A (HxD = 20 m × 20 m)					Tank B (HxD = 10 m × 20 m)				
Eigenmode	$t_r = 5t_c$	$t_r = 10t_c$	$t_r = 30t_c$	$t_r = 60t_c$	Eigenmode	$t_r = 5t_c$	$t_r = 10t_c$	$t_r = 30t_c$	$t_r = 60t_c$
1	112.2	110	112.2	120.8	1	141.2	139.6	139.6	185.3
3	114.4	111.9	113.3	121.1	3	141.8	139.9	139.9	186.1
5	123.8	121.5	120.5	122	5	163.3	161	161	212.1
Tank C (HxD = 40 m × 20 m)					Tank D (HxD = 20 m × 40 m)				
Eigenmode	$t_r = 5t_c$	$t_r = 10t_c$	$t_r = 30t_c$	$t_r = 60t_c$	Eigenmode	$t_r = 5t_c$	$t_r = 10t_c$	$t_r = 30t_c$	$t_r = 60t_c$
1	99.8	99.4	99.7	102.5	1	46.1	42.9	41.9	42.57
3	103.1	102.7	103.1	106	3	46.2	43	42	42.6
5	107.9	107.5	107.8	110.8	5	49.9	46.7	45.7	46.3

The steel tank is fixed at the base. The thermal loading is actually imposed as fixed nodal temperature, using the temperature pattern already described in Section 2 and no heat transfer takes place.

The self-weight of the conical roof is determined empirically based on several existing tank design reports. The used values are given in Table 2. These are average values and correspond to different types of roof, depending on the size of the studied tank. As it is clarified in the previous section, the case of roof failure is out of scope of this study. Furthermore, the *equivalent* thickness of the conical-shell roof is escalated in order to simulate roofs with different stiffness and consequently different restraint conditions for the cylindrical shell. It is noted that, even though the shell thickness of the conical roof is escalated, the self-weight of the roof remains the same. Furthermore, the roof self-weight is applied directly to the tank walls, in order to avoid buckling phenomena that may arise in the roof.

The size of the F.E. mesh should be carefully chosen to capture the possible buckling phenomena that may arise. Considering results of the literature ([19,20,21]) significant compression forces appear in the vicinity of boundaries and therefore a fine mesh is required in the corresponding regions to capture accurately the local buckling phenomena that may arise due. Thus, the discretization is selected to be non-uniform in order to decrease the total number of the finite elements and to avoid excessive computational cost. To this end, a mesh sensitivity study was conducted (included in Section 4).

4. Preliminary results - linear bucking analysis (LBA)

First, Linear Bucking Analysis (LBA) is conducted, aiming to evaluate the bucking modes and the critical temperature values. The steel is considered elastic and the coefficient of thermal expansion is assumed to be constant. The results of buckling analysis present a good approximation of the final failure mode and the possible global/local bucking phenomena.

Since there is no analytical solution for comparison with the numerical results, a mesh sensitivity study is performed. A denser mesh is adopted near the base and at the upper bound of the cylindrical shell (the dense mesh zone length near the boundaries is equal to 1.5 m). Regarding the circumferential direction, the reference mesh size is equal to 1° while in the vertical coordinate the loose mesh is 0.5 m and the refined mesh is 0.05 m. This mesh scheme is considered to be the reference case. The critical buckling temperature that results from the LBA of the reference case (for the first eigenmode) is compared to the respective critical values that result from analysis with different meshing schemes. The results are presented in Table 3.

It is concluded that as the meshing scheme becomes coarser, the temperature deviates from the reference critical temperature and the critical values are ascending. On the contrary, as the mesh (in both refined and non-refined regions) becomes denser, the results are very close to the reference case. Thus the meshing scheme of the reference case is adopted in this study. Additionally, the eigenmode for the meshing schemes 1, 2 and 3 (according to Table 3), is the same. It is pointed out, that the results of the mesh sensitivity study are in accordance with the outcomes corresponding study that is conducted in [19].

In LBA the incremental loading is the temperature pattern presented in Section 2. The gravity load is included in the initial conditions of the problem. Table 4 presents the critical buckling temperatures for all tanks, depending on the *equivalent* roof stiffness that is used. The

Fig. 2. 1st, 3nd, 5th and 7th buckling modes of fixed-roof Tank A.

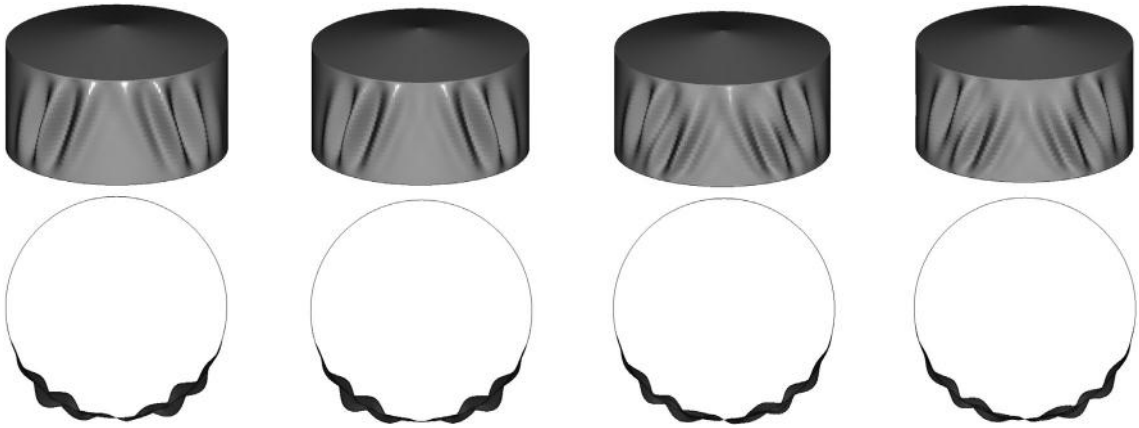

Fig. 3. 1st, 3nd, 5th and 7th buckling modes of fixed-roof Tank B.

buckling temperature is actually the temperature of the most heated meridian of the tank i.e. the meridian in the side of the incidence of fire. According to the results of the analyses, the eigenmodes appear in couples and the corresponding eigenvalues are identical e.g. the 1st and 2nd eigenvalues are the same, the 3nd and the 4th also etc. Therefore, only odd eigenvalues are included in Table 4. It is observed that for Tank A, C and D the critical buckling temperatures are not strongly influenced by the *equivalent* roof thickness. The only exception appears in Tank B for $t_r = 60t_c$, where the roof is very stiff. Tanks A, B and C (of same diameter) buckle for relatively low levels of temperature. Considering that steel starts to degrade after the 200 °C [34], the critical temperatures of Table 4 indicate that the most important parameter responsible for the instabilities that occur, is the thermal gradient. Tank B appears to have the best inherent fire-resistance, presenting the highest critical temperature. Concerning Tank D, which has the double diameter, the critical buckling temperature is very low in comparison to other tanks. This result can be attributed to the supplementary compressive load coming from the self-weight of roof.

Figs. 2, 3, 4 and 5 present the odd eigenmodes in plan and elevation (fire-side) views, for Tank A, B, C and D respectively. It appears that for Tanks A, B and D their first eigenmodes are similar. It is a global mode where the buckles are diagonal and antisymmetric with respect to the most heated meridian. The third eigenmode is symmetrical. On contrary, the eigenmodes for Tank C are local ones and buckles appear in the middle of the lower boundary of the cylindrical shell. Eigenmodes of higher order (7th), follow the pattern of the first one, but with additional buckles.

5. Numerical analysis techniques

The fire behaviour of the heated fixed-roof tank, is simulated through the finite element method. The problem is solved using non-linear transient thermal/structural numerical analysis. Actually the analysis comprises of a transient heat transfer pass and a static mechanical pass. A copy of the temperature field of the each increment is stored where a full thermal-structural solution is obtained and using this

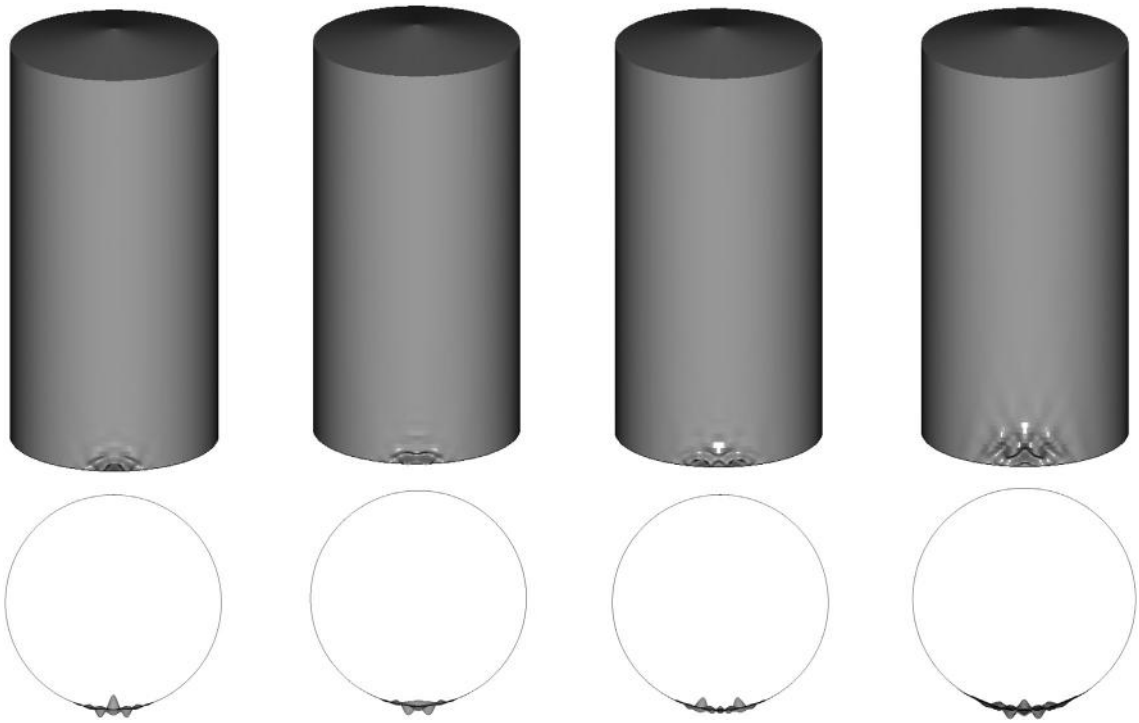

Fig. 4. 1st, 3nd, 5th and 7th buckling modes of fixed-roof Tank C.

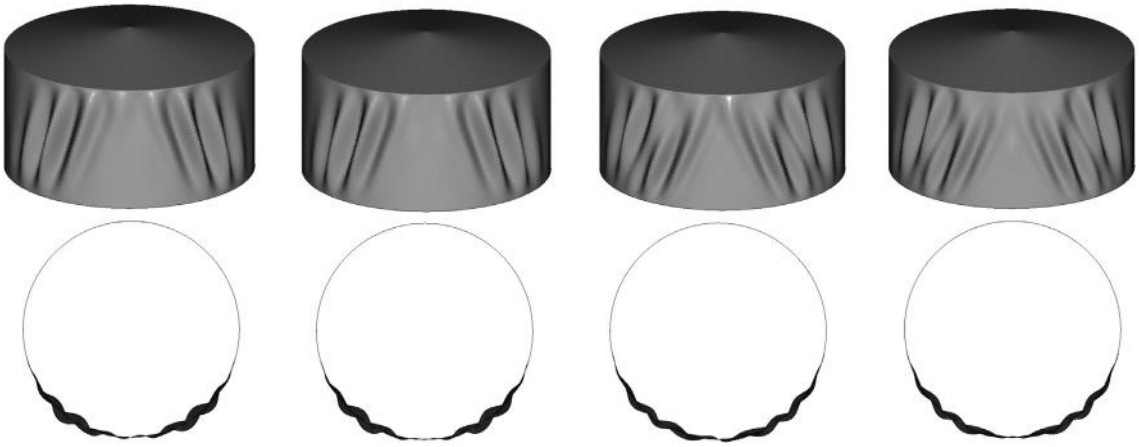

Fig. 5. 1st, 3nd, 5th and 7th buckling modes of fixed-roof Tank D.

temperature field to calculate the thermal strains in the next full thermal-structural solution increment. Moreover, large displacements are considered in the formulation of the mathematical problem. The numerical models are the same as described in the Section 3.

During the analysis, the temperature increases linearly through driven table input and the temperature of the most heated generator is the variable that replaces the load in the equilibrium path. For the empty tank the unique concurrent mechanical-static load is the self-weight. As is described in Section 2, the temperature profile of the heated tank is prescribed according to the thermal pattern and actually no heat transfer takes place. Specifically, the fixed temperature boundary condition is used in order to define the temperature-history for all nodes. The non-heated zone is assumed to be at zero temperature.

The arc-length method is utilized for the evaluation of the equilibrium path of the structural system and the AUTO STEP scheme, available in MSC Marc, is used. In this case, the primary control of the load step is based upon the number of recycles needed to obtain convergence. There is a number of optional user-specified criteria that can be used to additionally control the load step. It is noted that all the adaptive stepping procedure solution schemes (such as the Arc-Length method) are able to capture global instabilities but may not work efficiently when local instabilities occur (Kobayashi T. [35].), because the localized deformation energy which arises in local buckling phenomena is able to destabilize the iterative procedure scheme. In order to overcome this numerical problem the adaptive stepping procedure solution scheme is complemented with the Artificial Damping Technique ([36,37]).

The latter, practically stabilizes the adaptive iterative solution procedure and helps the corresponding algorithm to converge easily because it has the potential to find and handle the local buckling phenomena. This ability comes from the introduction of "artificial damping forces" in the equilibrium equations. More specifically, considering the equilibrium of a structure between the total external load P and the internal forces Q, the "artificial damping force F_D is also added and the following equation holds:

$$P - Q - F_D = 0 \tag{2}$$

where,

$$F_D = c \cdot M \cdot v \tag{3}$$

In Eq. (3) c is the damping ratio, M is an artificial mass matrix calculated for unit density and v is the vector of nodal velocities based on the nodal displacements. The damping ratio c is chosen appropriately (default value = 0.0002) in the first step of the iterative procedure, so as the damping energy to be only a very small part of the total deformation energy. Thus, the damping ratio c is actually the fraction of the dissipated energy to the total strain energy. Initially, as the structure deformes, the equilibrium of the system is stable and the values of the artificial damping forces (as well the damping energy) are small enough compared to the internal forces Q (and the total strain energy). Therefore, in this case the artificial damping energy is not affecting the overall behaviour of the system. In case where a local buckling phenomenon occurs in some region of the structure, the displacements of the nodes in this area are increased. The increase in the amount of strain energy which corresponds to these displacements is actually damped by the artificial damping energy which is also increased due to the fact that the corresponding nodal velocities are increased. Consequently, the moment that the local buckling occurs the value of the damping ratio will rapidly change, indicating that local buckling takes place.

The actual amount of damping energy is available on the post file as a global variable. By comparing the estimated (damping) energy with the actual values, the time increment is either increased or decreased. In this paper it is concluded that the artificial damping energy based time stepping scheme is very sensitive to the magnitude of the damping ratio that is initially defined in the analysis parameters. Thus, the user should conduct trial analyses for the right consideration of this parameter. If this value is very small, numerical instabilities and convergence problems may arise which may lead to confusing termination of the analysis.

6. Detailed study for Tank A through geometric non-linear analysis (GNA)

6.1. Tanks without initial imperfections

In this section the buckling behaviour of Tank A under non-uniform heating is studied thoroughly. In the following, the *equivalent* thickness of the roof, which actually describes the boundary conditions at the upper end of the shell is considered as $t_r = 10t_c$, where $t_c = 10\ mm$ is the shell thickness. First, trial analyses are conducted for the determination of the magnitude of the damping ratio. According to the results (Table 5), as the damping ratio decreases, the critical buckling temperature increases and finally converges to a certain value. Thus, for Tank A the damping ratio is chosen equal to 10^{-7}. Similar series of analyses were conducted for tanks with various *equivalent* roof thickness and was finally concluded that the same value can be used in all the analyses.

Table 5
Evolution of critical buckling temperature of Tank A as the damping ratio decreases.

Damping ratio	10^{-4}	10^{-6}	10^{-7}	10^{-10}
Critical buckling Temperature (°C)	133.3	142.32	143.27	143.27

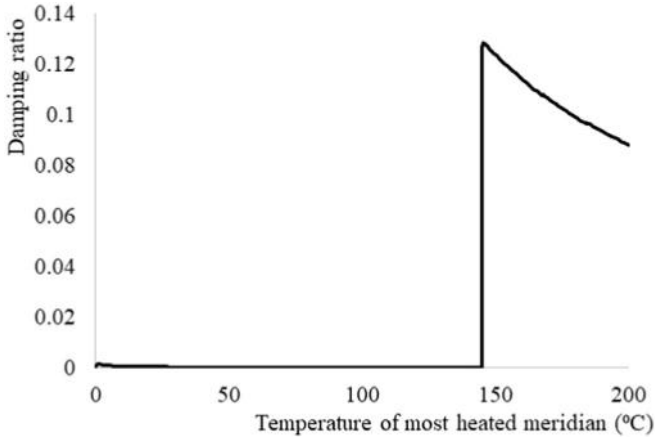

Fig. 6. Evolution of damping ratio with the temperature of the most heated meridian for Tank A ($t_r = 10t_c$).

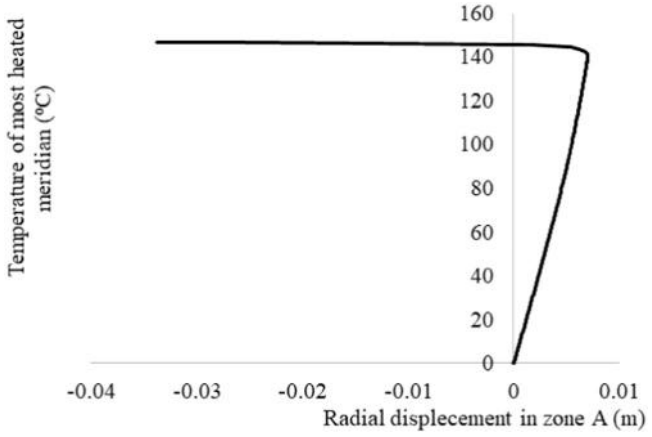

Fig. 8. Temperature vs. radial displacement curve for a node in the buckle region (zone A).

Fig. 6 presents the evolution of the damping ratio (the ratio of the damping energy to the total strain energy) with respect to the maximum temperature that is recorded on the tank (the temperature of the most heated meridian). This diagram indicates that when the temperature becomes equal to 143.5 °C, the damping ratio increases rapidly and this happens due to the instability that appears in the tank. This is also illustrated in Fig. 7 where the deformed shape of the tank is presented, before and after buckling. Moreover, the radial displacement of a random node in region A (as it is indicated in Fig. 7) is plotted in Fig. 8. In this diagram it is confirmed that for temperature equal to 143.5 °C, the radial displacement increases rapidly i.e. the shell buckles and the behaviour becomes non-linear.

It can also be noted that the deformed configuration of the heated tank at the buckling and post-buckling stages (Fig. 7) is dominated by the first buckling mode. During the post-buckling stage the geometry of the cylindrical shell becomes complicated and large displacements can be detected at the crest of the buckles. Actually, the instability that takes place is the result of both meridional and circumferential stress. The differential thermal expansion due to the temperature pattern in the circumferential direction generates the circumferential stresses. Moreover, meridional compression forces arise due to the restrained thermal expansion. The restriction is introduced by the fixed-roof and therefore the meridional stresses are dependent on the boundary conditions introduced by the roof.

It should be pointed out that the buckling temperature ($T_{cr} = 143.5$ °C) predicted using geometric non-linear analysis (GNA) is larger compared to the corresponding critical temperature that results from LBA (Tcr = 110 °C). This is a contradiction to the well-known trend of the mechanical loading of shells, where the buckling load that results from GNA is below the corresponding value of LBA. This paradox has been also reported in the literature ([16,17,37]). The inconsistency is explained through the "barrel effect" as it is referred in the study of Ross [16]. In this study it is reported that, the initially straight generators of the cylinder become curved during heating due to the effect of thermal expansion coefficient. The ensuing curvature is particularly important and results to a non-linear behaviour during the pre-buckling stage. Because of the continually increasing deflection of the initially straight generators, the load-bearing capacity of the cylindrical shell reduces and this results to the higher critical buckling temperature. The barreling effect and the resulting non-linear behaviour during the pre-buckling stage are generally accepted as an explanation of the thermal buckling paradox. The latter is also depicted in Fig. 8, where it is observed that during the pre-buckling stage, the behaviour is not linear.

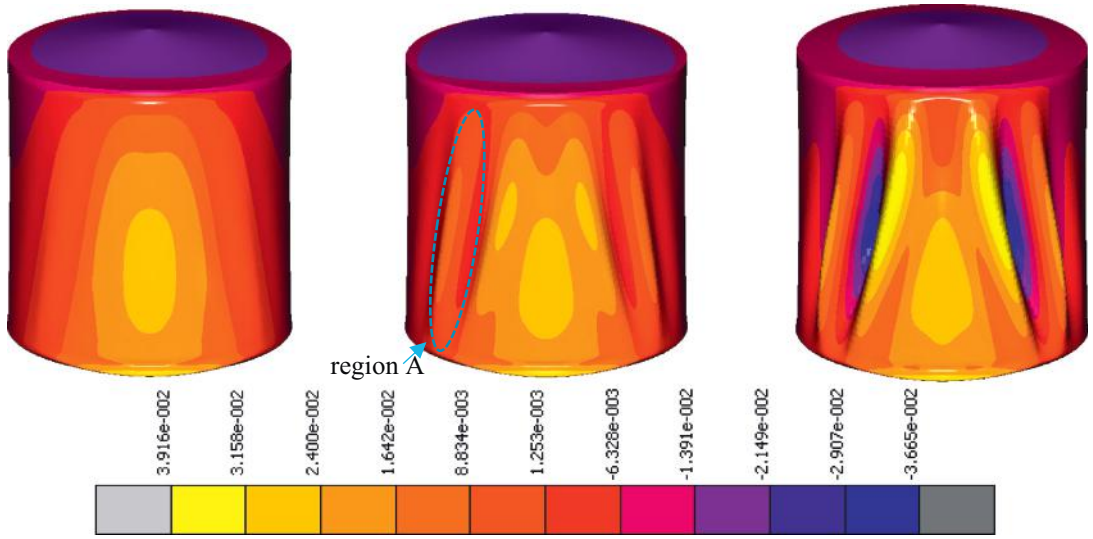

(a) pre-buckling state (T=142.5 °C) (b) buckling state (T= 143.5 °C) (c) postbuckling state (T=146.5°C)

Fig. 7. Radial displacement field and the deformed configuration of Tank A ($t_r = 10t_c$) before and after buckling.

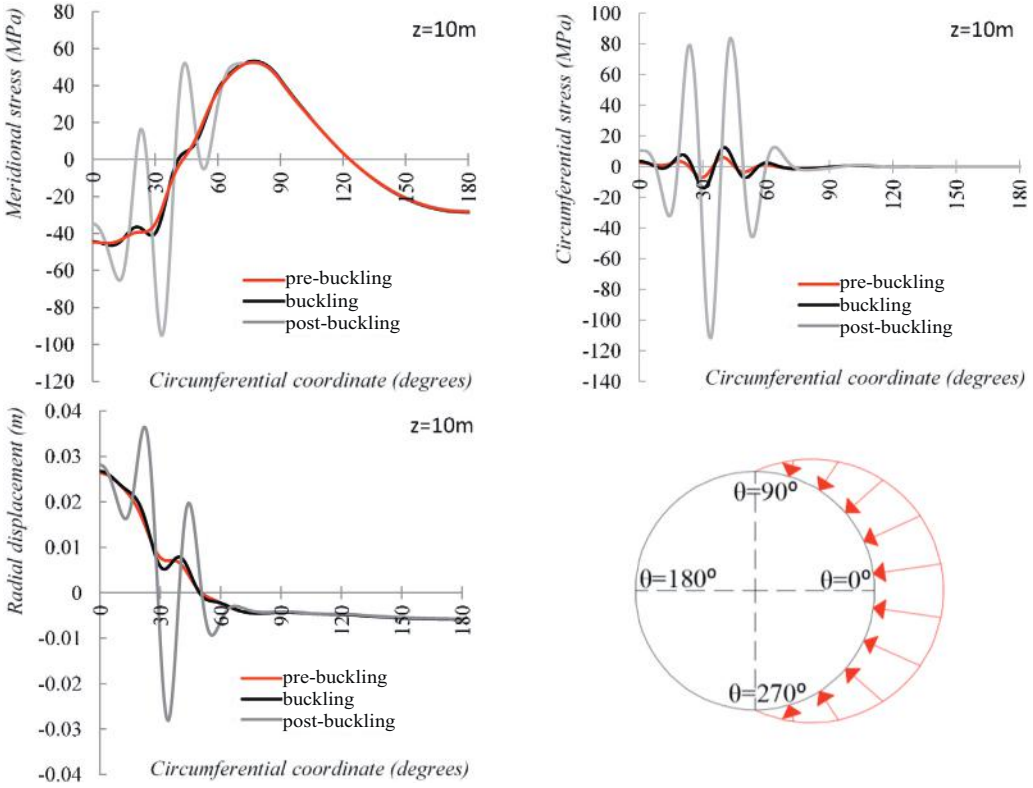

Fig. 9. Radial displacement, meridional and circumferential stresses at z = 10 m before and after the buckling.

In order to explain the complicated phenomena that arise in the heated tank, the components of the Cauchy stress tensor are plotted for various paths along the cylindrical shell. Fig. 9 presents the radial displacements and both the circumferential and meridional stresses around the circumference of the cylindrical tank at the mid-height (z = 10 m), before and after buckling. Specifically, half of the circumference is plotted since the phenomenon is symmetric with respect to the most heated meridian. In $\theta = 0^o$ lies the most heated generator, while in $\theta = 180^o$ the opposite generator is allocated to the side of the tank that is not heated i.e. the interval $270^o \le \theta \le 90^o$ corresponds to the heated region and for $90^o \le \theta \le 270^o$ the tank is at ambient temperature. It is observed that during the pre-buckling stage the meridional stresses are almost ten times larger than the circumferential ones (Fig. 9).

The stress state condition (due to heating) in the studied problem is self-equilibrated therefore, the stress pattern in both meridional and circumferential direction, changes between tension and compression so that the balance is maintained. During the post-buckling stage, both the circumferential stresses and radial displacements increase rapidly (Fig. 9). Also it is detected that in various locations e.g. at $\theta = 15^o$, $\theta = 30^o$ and $\theta = 45^o$ (which are allocated at the crest of the buckles) the radial displacements suddenly jump. After buckling, the meridional stresses decrease in the regions where the instability occurs (due to the fact that in these regions the shell area loses its load-carrying capacity in the meridional direction), while at the same time the circumferential stresses are remarkably increased due to the buckled shape which activates the load-carrying mechanism of the shell in the circumferential direction (catenary or tensile membrane action).

The stress field before and after instability is analogous to the corresponding one that appears in the case of an axially compressed plane membrane when it has an initial curved geometry or is subjected to transverse loading. In the case studied, the thermal bowing introduces the previous corresponding deformation.

Furthermore, Fig. 10, illustrates the radial displacement and both the components of the stress tensor along the circumferential direction for the pre-buckling, buckling and post-buckling stages at different levels (horizontal sections) along the height of the cylindrical shell. It is clear that before buckling, the meridional stresses are maximized near the lower boundary of the cylindrical shell (z = 2.5 m) and the same happens after buckling. On the other hand, the circumeferential stresses are larger near the mid-height of the shell.

The meridional stress pattern along the height of the tank for different heated generators ($\theta = 0^o$ and $\theta = 45^o$) of the cylindrical shell and the corresponding distribution of radial displacements are plotted in Fig. 11. Before buckling and close to the critical temperature, the variation of meridional stress along the height of the generators is almost linear except the upper and the lower base of the tank. In these zones, large compressive and tensile stresses are detected locally, due to the constraint provided by the fixed boundary and the roof of the tank respectively. After buckling, the distribution of meridional stresses becomes non-linear and important compressive forces take place in the body of the cylinder (i.e. far from the upper and lower regions of the tank). Regarding the radial displacements, it can be observed that after buckling, the maximum values are recorded in a zone above of the mid-height of the tank for the most heated generator and this zone is transferred downwards in the less heated generators.

6.2. Imperfect tanks

Aiming to a more realistic assessment of tank's fire behaviour, initial imperfections are incorporated in the geometry of the cylindrical shell in this paragraph. There are many different ways to introduce initial geometric imperfections in the context of finite element analysis. A simple way is to extract the buckling eigenmodes and introduce them as imperfections with a specific amplitude. Thus, in this study, the normalized buckling modes are multiplied by a scale factor, leading to

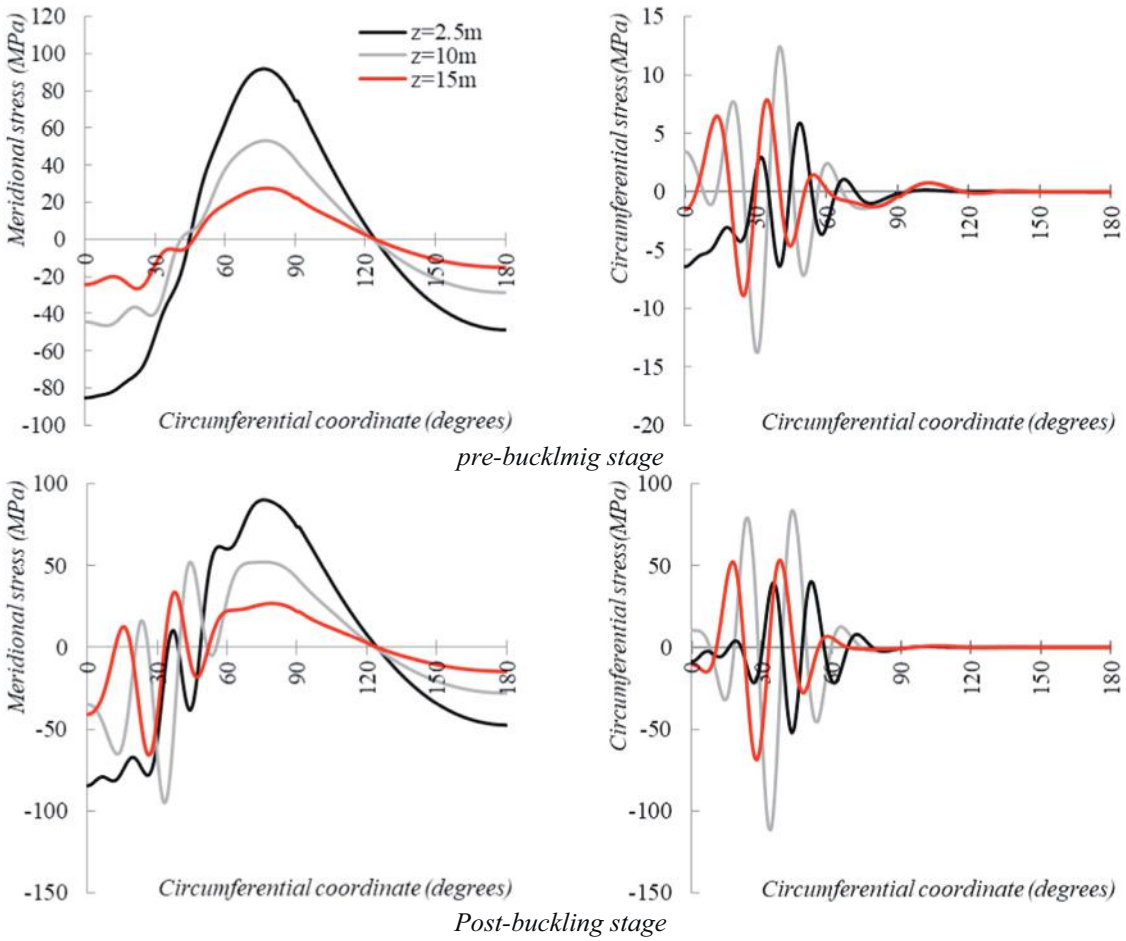

Fig. 10. Comparison of radial displacement, meridional and circumferential stresses at various levels of height before and after the buckling.

the desired maximum amplitude and the resulting buckled geometry is added to the initial coordinates of the structure.

The current regulations do not give special guidelines for the case of thermal loading of fixed-roof tanks and there are no standards for the shape and the magnitude of initial imperfections that should be considered in the study. Therefore, this study only aims to the parametric investigation of the effect of the geometric imperfections to the behaviour of heated tanks. Here, the 1st and the 7th eigenmodes are used. The 1st eigenemode is antisymmetric while the 7th is symmetric with respect to the most heat meridian.

First, parametric analyses are conducted for the determination of the magnitude of damping coefficient and the value where the critical bucking temperature is converged is equal to 10^{-10}. This value is chosen for the numerical model that includes also the 7th eigenmode. Fig. 12 summarizes the results of the imperfection sensitivity study in terms of critical buckling temperature.

6.2.1. Initial imperfections extracted from 1st eigenmode

In case where the maximum amplitude of initial imperfections used in the analysis is 2 mm, the failure bulking mode is illustrated in Fig. 13 during the buckling and the post-buckling stages. At the buckling stage, the deformed shape of the tank is dominated by the 1st eigenmode, but in the next step of the analysis for minor increase of temperature (0.005 °C) the deformed configuration changes simultaneously and local buckling occurs at the base of the cylindrical shell. The final failure mode is similar with the 5th eigenmode that comes from the LBA. Actually, the critical temperature consists a bifurcation point. The imperfect cylindrical shell finally buckles at $T_{cr} = 124.3$ °C, which is approximately 20 °C less than the critical buckling temperature that results when the model is considered to be perfect (Section 6.1). The post-buckling stage is stable and multiple local buckling instabilities appear near the base of the tank. The results of the parametric analyses for the stiffness of the roof, indicate that both the critical buckling temperature and the failure mode are not affected.

On the other hand, as the amplitude of initial imperfections is escalated, the critical buckling temperature decreases and it is observed that the failure buckling mode is sensitive to the boundary conditions induced by the roof of the tank. The results of the parametric analyses for maximum amplitude of initial imperfections equal to 5 mm, show that for *equivalent* roof thickness $10t_c \le t_r \le 30t_c$, the failure mode is very similar to the configuration described in Fig. 13, but for $50t_c \le t_r \le 60t_c$ the deformed configuration changes and local buckling takes place approximately at the mid-height of the cylindrical shell (Fig. 14). The failure mode is not-symmetric and in the post-buckling stage successive local buckling appear at the base of the tank. On the contrary the critical bucking temperature remains almost unchanged as the *equivalent* thickness of the roof increases.

For further increase of the maximum amplitude of initial imperfections (10 mm), the critical buckling temperature decreases further and remain approximately constant as the *equivalent* roof thickness increases. The failure mode that appears for all the parametric analyses for the different boundary conditions induced by the roof is presented in Fig. 15.

6.2.2. Initial imperfections extracted from 7th eigenmode

In case where the 7th eigenmode is used for the incorporation of the initial imperfections, the failure mode is very similar to the first bucking

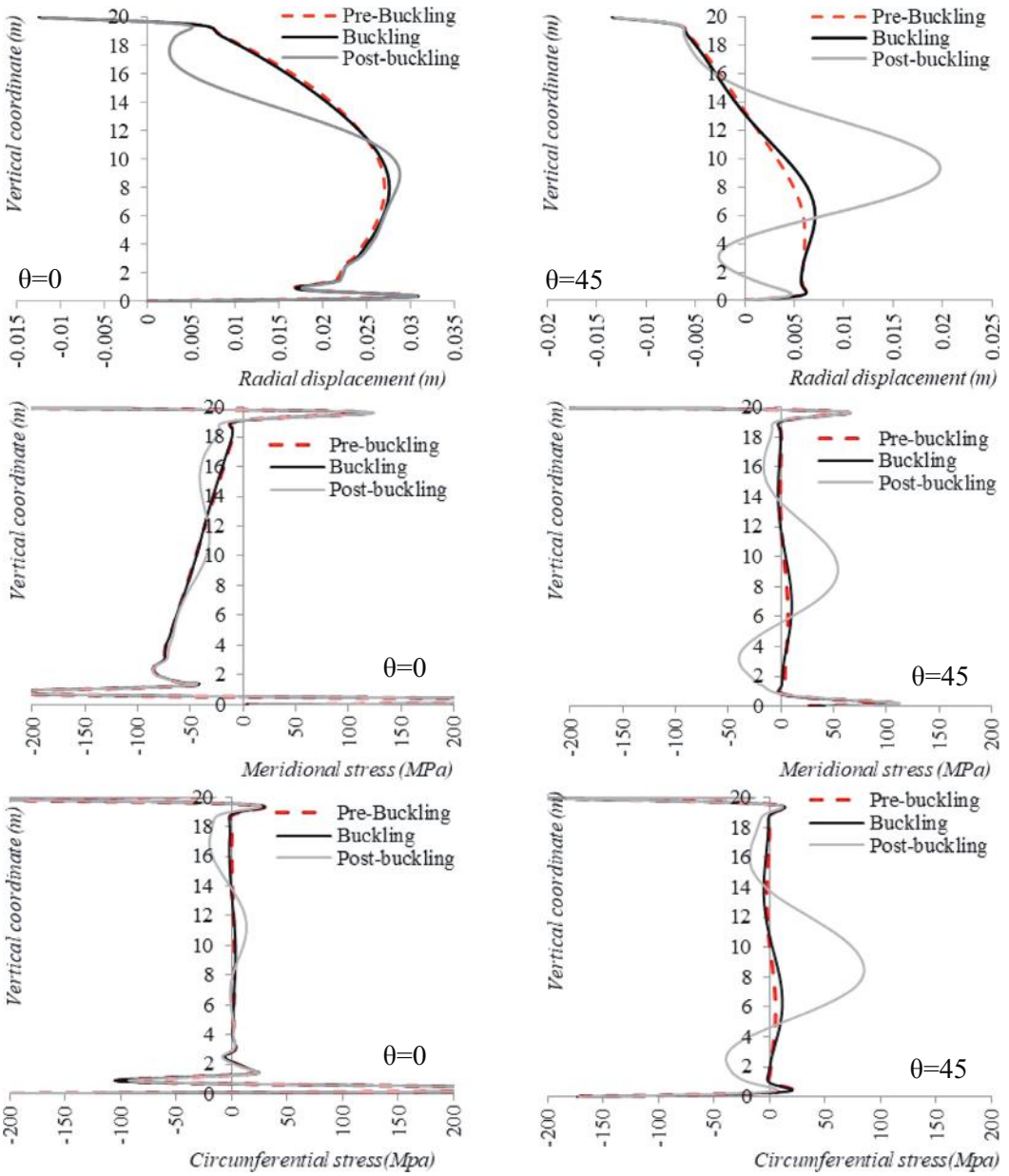

Fig. 11. Radial displacement, meridional and circumferential stresses along generators of the cylinder in heated zone ($\theta = 0°$ and 45°).

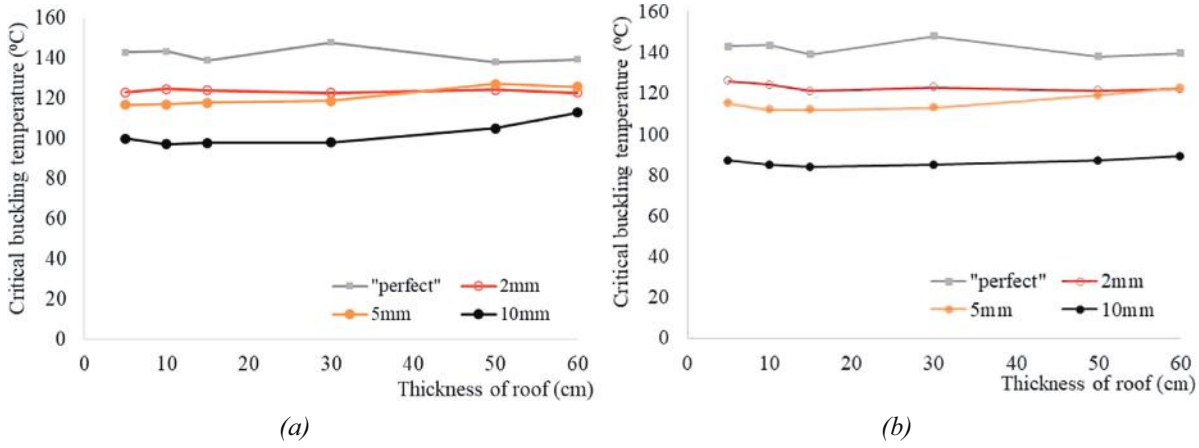

Fig. 12. Variation of critical buckling temperature with the equivalent thickness of roof and for different amplitudes of initial imperfections using (a) 1st eigenmode and (b) 7th eigenmode.

Fig. 13. Deformed configuration of Tank A before and after buckling (amplitude of initial imperfections 2 mm).

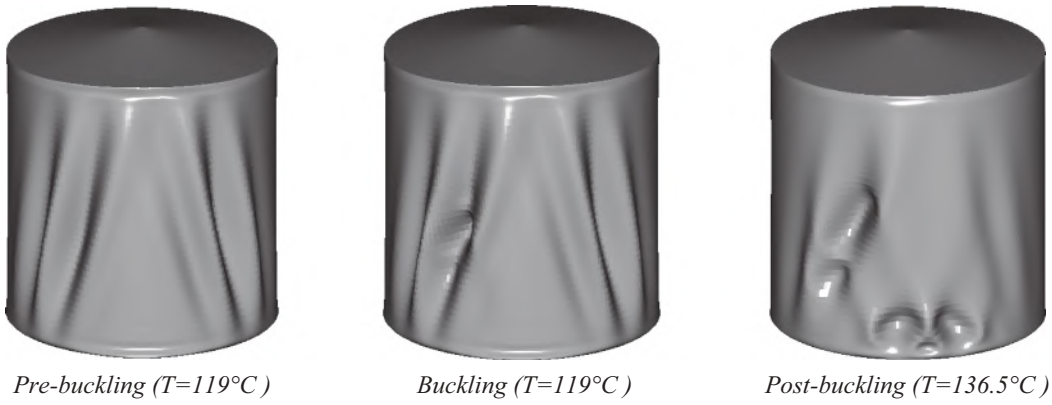

Fig. 14. Deformed configuration of Tank A before and after buckling (amplitude of initial imperfections 5 mm).

mode and this is valid as the amplitude of the initial imperfection is escalated as well for all the parametric analyses considering different *equivalent* roof thicknesses.

All the previous indicate that the critical buckling temperature is very sensitive to the amplitude of the initial imperfections (reduction up to 39% for the case where the amplitude is 10 mm). Moreover, the final failure mode is complicated due to the existence of several possible post-critical solutions and depends on the shape of the geometric imperfections, their amplitude and the system used for the roof.

7. Buckling behaviour of fixed-roof tanks with various slendernesses

7.1. Unstiffened tanks

This section presents a detailed study for the effect of slenderness (ratio of height to diameter) of cylindrical shell to the fire behaviour of tanks under non-uniform heating. Three different cases are examined (Tanks B, C and D), as they are presented in Section 2. In the same time, the effect of *equivalent* roof stiffness is studied. Is noted that in this part of the study, the numerical models do not include initial imperfections.

Fig. 15. Deformed configuration of Tank A before and after buckling (amplitude of initial imperfections 10 mm).

Table 6
Critical buckling temperature for tanks with different slenderness and for different equivalent thickness of the roof (°C).

	Slenderness	$t_r = 5t_c$	$t_r = 10t_c$	$t_r = 15t_c$	$t_r = 30t_c$	$t_r = 50t_c$	$t_r = 60t_c$
Tank A	1	143.0	143.5	138.8	147.8	138.0	139.4
Tank B	0.5	224.7	202.2	196.2	197.7	214.2	227.7
Tank C	2	100.0	99.0	89.0	99.3	130.4	115.8
Tank D	0.5	109.8	94.8	91.8	91.3	90.3	93.3

Table 6 summarizes the critical bucking temperature for all the case studies. In all cases, the critical buckling temperature is higher compared to the corresponding value that comes from the LBA. As it is anticipated, the less slender tank (Tank B) which at the same time has the smallest diameter, appears to have the better inherent resistance against the non-uniform heating loading. But, slenderness cannot be an absolute criterion for the classification of the inherent fire-resistance of the tanks. Although Tank D has the same slenderness with the previous one (but double diameter), buckles for lower temperature (almost half) in comparison with Tank B. This can be attributed to the additional self-weight of the roof of Tank D. Additionally, it is clear that the critical buckling temperature decreases as the slenderness of the cylinder is escalated. The comparison is more accurate when the first three tanks are considered, since their diameter remains the same.

For the study of Tank B, the damping coefficient was taken equal to 10^{-8}, since for this magnitude the critical buckling temperature has already converged. The deformed configuration of the tank (for the case where $t_r = 5t_c$) during, before and after buckling, is illustrated in Fig. 16. As the temperature increases, the cylindrical shell expands in both the meridional and circumferential directions. When the temperature of the most heated meridian becomes equal to 224.73 °C, the tank buckles (Fig. 16) and the deformed shape follows the 1st eigenmode of the tank. But due to the fact that the equilibrium mode is unstable, the cylindrical shell jumps to a more stable path as illustrated in Fig. 16. Actually, the critical temperature is a bifurcation point from an unstable antisymmetric eigenmode to a stable one. According to the results of the parametric analyses, with respect to the thickness of the roof shell, the failure mode is not affected by the stiffness of the roof. Moreover,

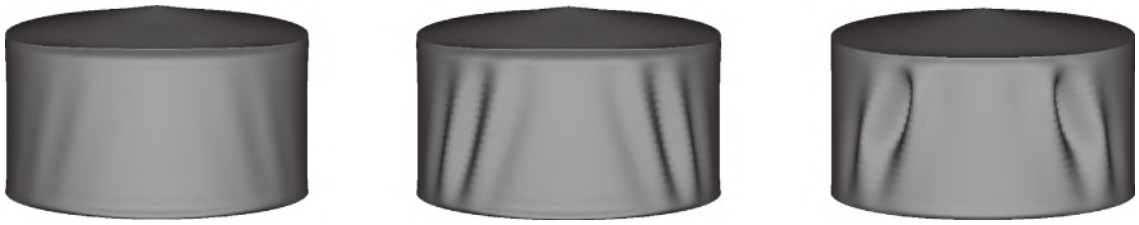

Fig. 16. Deformed configuration of Tank B before and after buckling.

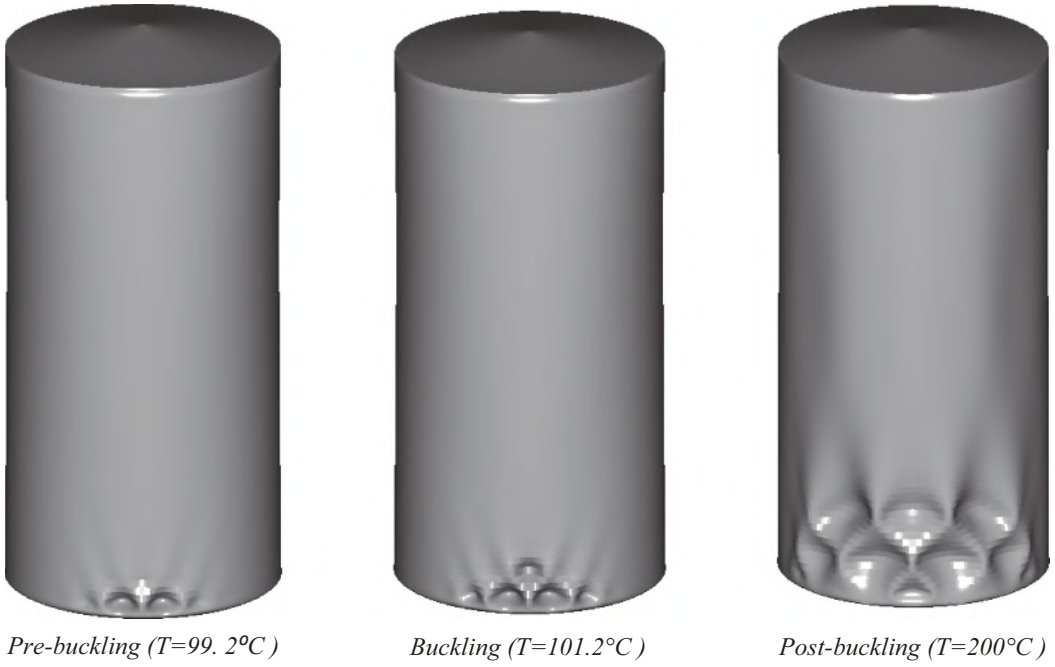

Fig. 17. Deformed configuration of Tank C before and after buckling.

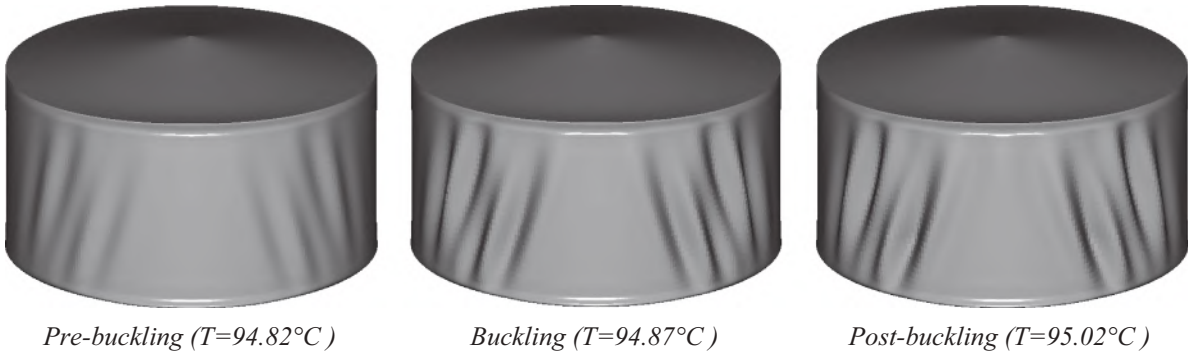

Fig. 18. Deformed configuration of Tank D before and after buckling.

Table 7
The wall thickness of the cylindrical shell (in cm) for all three cases examined.

Case	Zone A	Zone B	Zone B	Zone D	Zone E	Zone F	Zone G	Zone H	Zone I
SW1	1.77	1.57	1.37	1.17	0.97	0.78	0.64	0.64	0.64
SW2	1.77	1.57	1.37	1.17	1.00	1.00	1.00	1.00	1.00
SW3	2.00	2.00	1.50	1.25	1.15	1.00	1.00	1.00	1.00

the critical buckling temperature slightly changes depending on the degree of restraint induced by the roof (Table 6).

In the case of Tank C, the damping ratio was chosen to be equal to 10^{-10}, based on the results of trial analyses. According to the findings of the parametric study, considering the induced restraint due to the roof, the buckling failure mode of tanks is not affected, and the critical buckling temperature slightly changes. The deformed configuration of the tank during heating is illustrated in Fig. 17. The deformed shape follows the 6th buckling mode according to the results of LBA i.e. local bulking appears near the base of the cylindrical shell. The post-buckling path is stable and the buckles spread as the temperature increases. Finally, the buckling failure mode of Tank D (damping ratio 10^{-8}) is illustrated in Fig. 18 which is a global mode with diagonal buckles (similar to the 1st buckling mode of Fig. 5). The same remarks, as for previous tanks, concerning the effect of the roof stiffness, hold in this case also.

7.2. Stiffened tanks

According to the previous detailed research, it is concluded that the critical buckling temperature in all cases lies between 100° and 220 °C approximately and the failure is due to elastic buckling. For this temperature range, the reduction of the modulus of elasticity of steel is negligible. Thus the degradation of materials properties due to increased temperature seems to have little influence on the failure of the tanks. Therefore, the following study examines if the usual stiffening techniques that are used at ambient conditions for other types of loading like wind, earthquake etc., are beneficial for the type of thermal loading that is studied in this paper.

7.2.1. Stiffening methods

Three different types of stiffening methods are examined herein. The first method uses horizontal stiffening rings i.e. in the plane section of the cylindrical shell. Three different layouts are studied for every tank and the rings are placed every 4 m, 2 m and 1 m (internal-vertical distance) in each case respectively. The second method uses stiffeners along the vertical direction of the cylindrical shell. In the sparse layout

Table 8
The critical buckling temperatures (°C) for the stiffened Tank A.

	Horizontal rings			Vertical stiffeners		Stepwise thickness		
Reference case (unstiffened tank)	4 m	2 m	1 m	30°	15°	SW1	SW2	SW3
143.5	142.8	152.8	597.9	141.8	159.2	93.4	116.8	99.4

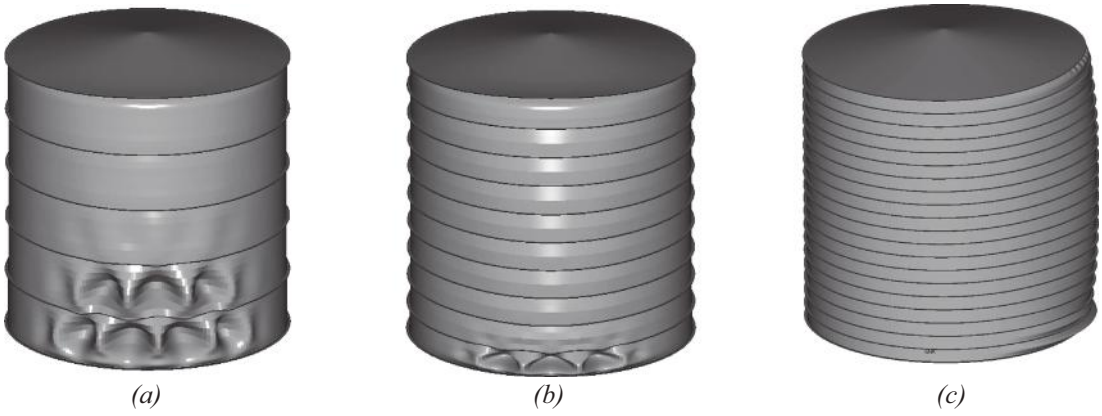

Fig. 19. The failure modes of Tank A for horizontal rings every (a) 4 m, (b) 2 m and (c) 1 m.

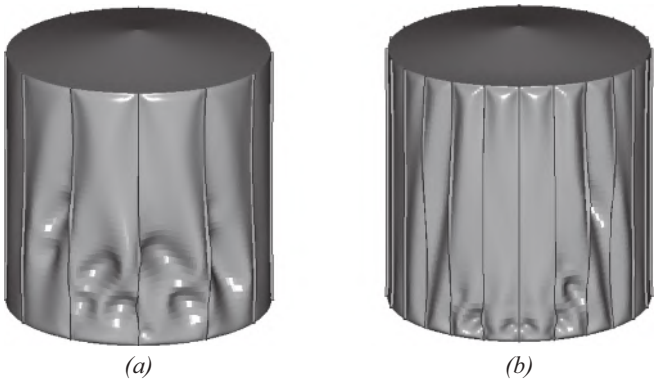

Fig. 20. The failure mode (front view) of Tank A for vertical stiffeners every (a) 30° and (b) 15°.

the vertical stiffeners are placed every 30° around the cylindrical shell while in the most dense case, every 15°. In all cases the stiffeners (both horizontal and vertical) consist of plates 15 cm wide while the thickness is equal to 15 mm. The stiffeners are simulated using shell elements incorporated in the numerical models described in Section 3. Concerning the third stiffening method, stepwise thickness along the height of the tank is considered. The cylindrical shell is discretized in 9 zones, in the vertical direction, and the thickness of the cylindrical shell is escalated from larger to smaller values. Three different cases are examined as it is presented in Table 7.

The next section presents the results for the all the tanks with different slenderness values that are studied in this paper. All the numerical analyses are conducted according to Section 5 and the models are perfect (i.e. no geometric imperfections are taken into account) in this part of the paper. First, the trial analyses concerning the value of the damping ratio are conducted and the value 10^{-7} is adopted for all tanks. Furthermore, it is noted that the *equivalent* roof thickness is considered equal to 10 cm in all the analyses hereafter.

7.2.2. Stiffened Tank A

Table 8 summarizes the critical buckling temperature for all different stiffening methods that are examined, for Tank A. In the case where the horizontal rings are used every 4 m, the critical buckling temperature is almost the same with the reference case where the tank is unstiffened. When the rings are denser (every 2 m and 1 m), the critical temperature increases and this indicates that the horizontal rings are effective for the non-uniform heating loadcase. Fig. 19 illustrates the failure mode for Tank A in the case where horizontal rings are used. Without exception the tanks fail due to local bucking at the base of the cylindrical shell. When the horizontal rings are sparse, the local buckling first takes place at the bottom of the tank and gradually spreads. But if the rings are placed more closer to each other, the phenomenon tends to be localized. In Fig. 19(c), the side view (the part of the circumference that corresponds to $180^{\circ} \le \theta \le 360^{\circ}$) of the tank is captured, in order to visualize in a better way the local buckling in the base of the cylindrical shell. It is seen, that the failure mode of the tank is different from that of the reference case and this can be attributed to the reduced buckling length due to stiffeners.

Fig. 20 presents the failure mode of the tank where vertical stiffeners are welded in the cylindrical shell. It is observed that the deformed configuration combines both the 1st global eigenmode of the unstiffened tank and local buckling in the base of the tank. This is valid for both layouts of the vertical stiffeners that were examined. In both cases, the buckles are confined between the vertical stiffeners

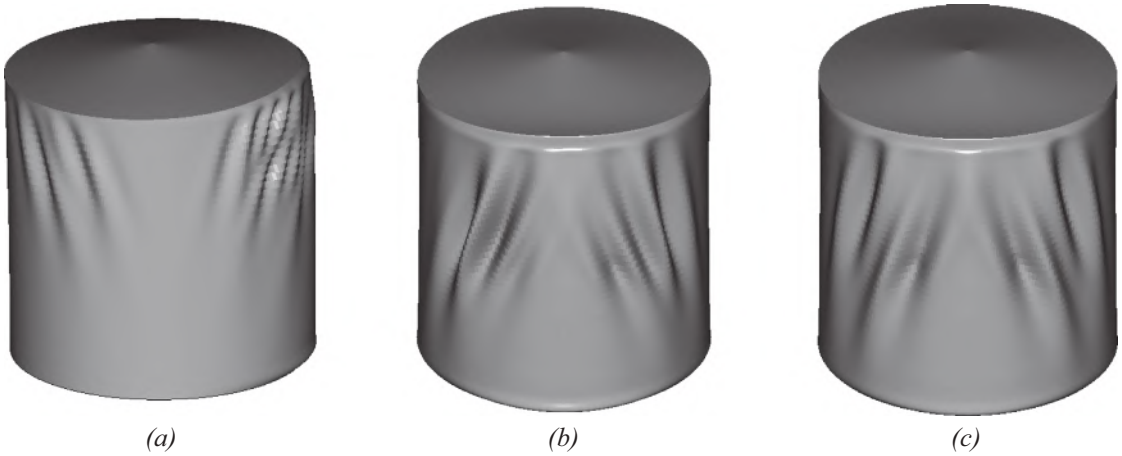

Fig. 21. The failure mode of Tank A for the stepwise thickness method (a) SW1, (b) SW2 and (c) SW3.

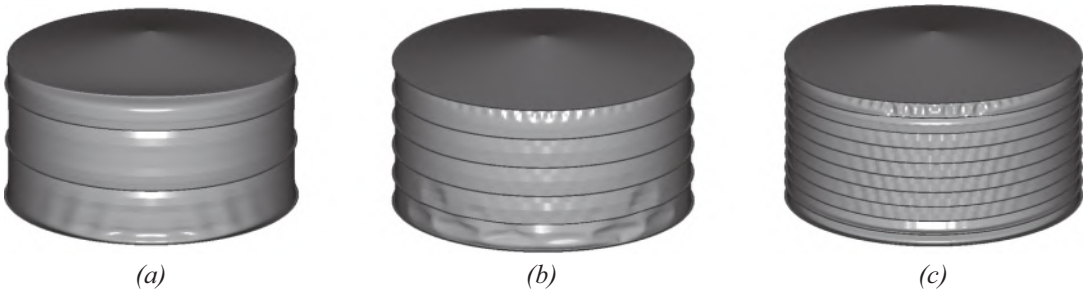

Fig. 22. The failure modes of Tank A for horizontal rings every (a) 4 m, (b) 2 m and (c) 1 m.

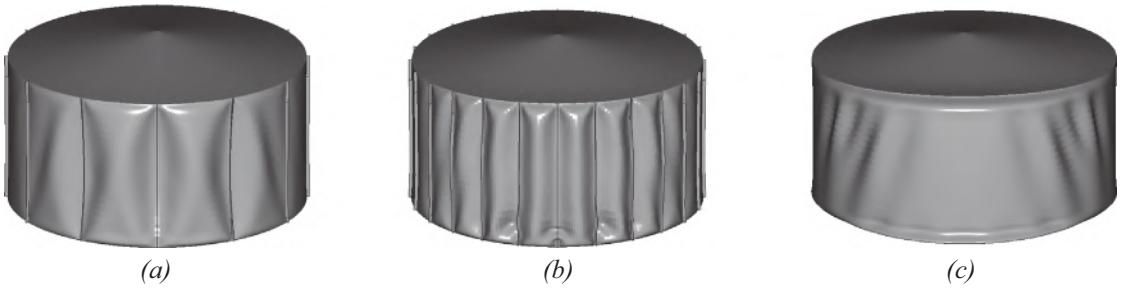

Fig. 23. The failure mode of Tank B for vertical stiffeners every (a) 30° and (b) 15° and (c) for the stepwise thickness method.

Table 9
The critical buckling temperature (°C) for the stiffened Tank B.

	Horizontal Rings			Vertical stiffeners		Stepwise thickness
Reference case	4 m	2 m	1 m	30°	15°	SW2
202.2	275.6	415.1	679.3	200.1	220	248.1

and the global buckling mode is still obvious. Actually the specific stiffeners reduce buckling length in the circumferential direction and this is not so beneficial since the global instability mode is governed mostly by waves with wave length larger in the meridional direction. For the first arrangement (stiffeners per 30°), the critical buckling temperature is almost the same with the reference case, but for the second one (stiffeners per 15°) increases. In general, the method of introducing vertical stiffeners slightly improves the resistance of the shell against the non-uniform heating load.

The failure modes for Tank A when the stepwise thickness stiffening method is used are illustrated in Fig. 21. In Fig. 21(a), the side view (the part of the circumference that corresponds to $180^{\circ} \le \theta \le 360^{\circ}$) of tank is captured, in order to visualize in a better way the deformed configuration of the cylindrical shell. In this case the buckling first takes place in the upper part of the tank (heated side) and afterwards in the backside. For the second and the third stiffening arrangements, the failure mode is very similar and is dominated by the first eigenmode of the reference tank. The critical buckling temperature for these stiffening methods is lower with respect to the reference case (Table 8). Thus, it is concluded that for this type of stiffening, although it is widely used at ambient temperature for other types of loading, is not appropriate for the non-uniform heating load, in the case of Tank A.

It is noted that the stepwise methods SW1 and SW3, in all cases led to reduction of critical buckling temperature and the results are not presented for the rest of the tanks.

7.2.3. Stiffened Tank B

Tank B has the better inherent resistance in comparison to the rest of the tanks since it is less slender. The failure modes of Tank B for all the cases that were examined, are presented in Figs. 22 and 23. The majority of examined stiffening methods are proved to be beneficial and the behaviour of the tank is enhanced since the critical buckling temperature is increased with respect to the reference case (Table 9). The only exception is the case of the vertical stiffeners per 30°, where the critical buckling temperature is almost the same with the reference case. When the horizontal ring stiffening method is used, local buckling appears in the lower base of the cylindrical shell. For the more dense rings (every 1 m), local buckling also appears in both lower and upper heated part of the shell and the buckling temperature increases almost 300%. In contrast with Tank A, in case of vertical stiffeners the global buckling mode does not appear and only local buckling takes place in the lower base of the heated side of the cylindrical shell. In case where the stepwise thickness scheme is included in the numerical model, the failure mode combines both the global and the local eigenmode and the critical buckling temperature of the tank slightly increases with respect to the unstiffened tank. Thus, it is concluded that the horizontal

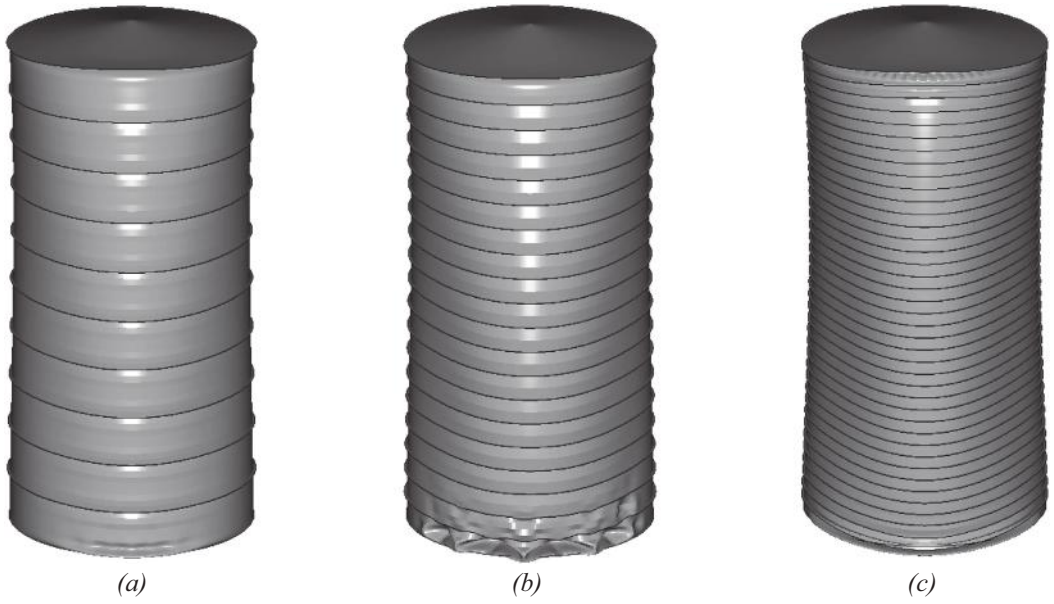

Fig. 24. The failure modes of Tank C for horizontal rings every (a) 4 m, (b) 2 m and (c) 1 m.

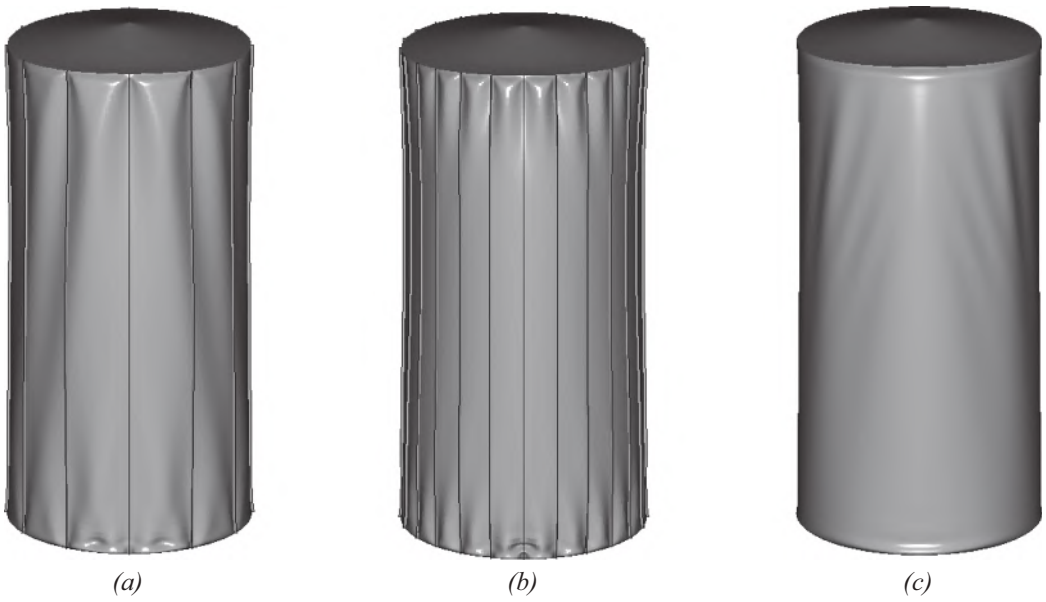

Fig. 25. The failure mode (front view) of Tank C for vertical stiffeners every (a) 30° and (b) 15^0 and (c) for the stepwise thickness method.

rings is the more efficient method for improvement of performance of this type of tank against the non-uniform heating load.

7.2.4. Stiffened Tank C

The same remarks, regarding the effectiveness of stiffening methods, are valid for Tank C also. The most efficient method is the horizontal rings per 1 m. In this case the critical buckling temperature is almost six times higher in comparison with the case of the unstiffened tank. The more sparse array of horizontal rings (every 4 m and 2 m) do not affect significantly the behaviour of the tank. The less reliable method is again the vertical stiffeners as it is also concluded in the previous. The stepwise thickness scheme slightly improves the resistance of the tank against the non-uniform loading. The failure modes of Tank C for all the cases that are examined are presented in Figs. 24 and 25 (see Table 10).

7.2.5. Stiffened Tank D

The horizontal rings is the most efficient technique for Tank D as well. When the rings are placed every 4 m, the cylindrical shell fails due to local buckling near the lower base of tank and then buckles appear to the top of the shell (Fig. 26 (a)). In this case, the critical buckling temperature slightly increases in comparison with the reference case. According to Table 11, when the rings are more dense, the resistance of tank against the non-uniform heating load, increases significantly. In this case, the local buckling of the cylindrical shell is observed near the upper base of the most heated side (Fig. 26(b)). In both cases the horizontal rings, contribute to the reduction of the buckling length of the shell, preventing the global failure mode and leading to local instabilities. For the case where horizontal rings are placed every 1 m, the analysis failed due to convergence at $T = 800$ °C and the final failure mode could not be captured.

On the other hand the vertical stiffeners does not contribute to the improvement of inherent fire-resistance of the tank, since the critical buckling temperature does not increase (Table 11). In both arrays (every 30° and 15°) the tanks fails due to the global failure mode (Fig. 27) which also appears in case of the unstiffened tank. Regarding the stepwise thickness method, the fire-resistance (in terms of critical buckling temperature) increases. It is interesting to notice that first the diagonal buckling appears only at the upper part of the cylindrical shell. As the temperature increases, the same happens at the back "cold side" also (Fig. 28).

Table 10
The critical buckling temperature (°C) for the stiffened Tank C.

	Horizontal Rings			Vertical stiffeners		Stepwise thickness
Reference case 99.0	4 m 113.7	2 m 113.7	1 m 626	30° 110.95	15° 119.5	SW2 139.3

8. Summary - conclusions

This paper addresses the problem of the fire-behaviour of thin-walled tanks with fixed roofs under non-uniform heating that may be generated in case of a neighboring fire-engulfed tank. The thermal pattern proposed in Liu [19], is used for the simulation of the non-uniform thermal loading. The study is focused on the case of an empty tank, since the presence of liquid has beneficial effect on the structural stability phenomena that appear. Four tanks of different geometry are studied.

First, the behaviour of Tank A is studied in detail. It is found that as the temperature increases the shell tends to expand both in meridional and circumferential directions. The restraint to the thermal expansion induced by the fixed base and the roof, generates stresses which (both tensile and compressive) around the circumference so that they balance each other. The meridional compression forces are higher than the circumferential ones and they trigger the instability of the thin-walled cylindrical shell. The fixed-roof tank fails for critical buckling temperature equal to 143.5 °C where the global elastic buckling occurs.

Fig. 26. The failure modes of Tank D for horizontal rings every (a) 4 m and (b) 2 m.

Table 11
The critical buckling temperature (°C) for the stiffened Tank B.

	Horizontal Rings		Vertical stiffeners		Stepwise thickness
Reference case	4 m	2 m	30°	15°	SW2
94.8	118.8	658	93.3	99.2	133.23

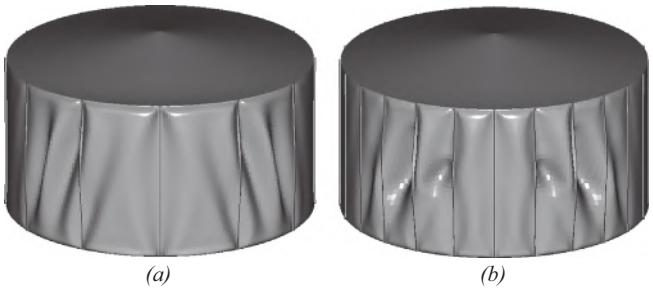

Fig. 27. The failure mode of Tank D for vertical stiffeners every (a) 30° and (b) 15°.

Aiming to a more realistic study of the behaviour of tanks against non-uniform heating, initial geometric imperfections were incorporated in the cylindrical shell. A parametric study with respect to the shape of the imperfect shell and the maximum amplitude of imperfections is conducted. It is found that the consideration of initial imperfection affects significantly the fire-behaviour of fixed-roof tanks. The effect is obvious in both the final failure mode and in the magnitude of critical buckling temperature. Specifically, as the amplitude of initial imperfections increases the critical buckling temperature considerably decreases. This is more intense in case where high-order eigenmodes are used for modeling the initial imperfections. Furthermore, the effect of the roof stiffness of tanks to their structural stability is examined. It is concluded that the roof *equivalent* stiffness does not affect the magnitude of the critical buckling temperature but the final failure mode of the cylindrical shell can be altered, depending on the boundary conditions on the roof.

The study of tanks with different geometry, reveals that their fire-behaviour depends both on the slenderness and diameter of the cylindrical shell. For all cases the thermal buckling occurs for relatively low temperature temperatures (between 100 °C και 250 °C). It is found that the critical buckling temperature decreases as the slenderness of the cylindrical is escalated. But the self-weight of the roof is also an important factor that affects the structural stability of thin-walled tanks and this can be attributed to the supplementary compression forces that are introduced. The less slender tank which in the same time has the smallest diameter, appears to have the better inherent resistance against the non-uniform heating loading.

Finally, the effectiveness of stiffening techniques that are used at ambient conditions, are beneficial for the type of loading. It is found that the horizontal rings are the most efficient technique for improvement of the inherent fire-resistance of tanks. Depending on the arrangement of the rings and on the geometry of the tank, the critical buckling temperature can be significantly increased. The stepwise thickness method that is widely used at ambient temperature for other types of loading, is not very effective for the non-uniform heating load and the vertical stiffeners are proved to be inefficient for improvement of the fire-performance of fixed-roof tanks.

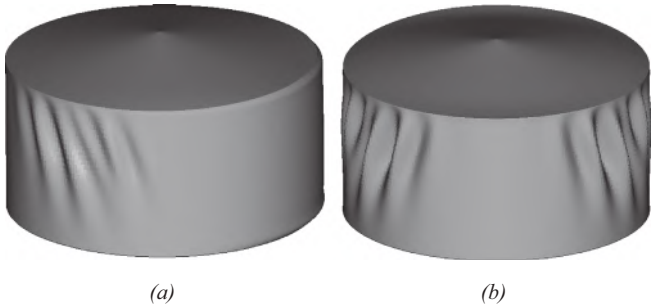

Fig. 28. The failure mode (front view) of Tank D for the stepwise thickness method (a) side and (b) front view.

References

[1] API STD 650:2013, Welded Tanks for Oil Storage, 12 ed. American Petroleum Institute, 2013.
[2] NFPA 30:2012, Flammable and Combustible Liquids Code, National Fire Protection Association, Quincy, MA, USA, 2012.
[3] H. Persson, A. Lönnermark, Tank fires review of fire incidents 1951–2003, BRANDFORSK Project 513-021, SP Fire Technology, SP REPORT, 2004:14.
[4] E. Brunesi, R. Nascimbene, M. Pagani, D. Beilic, Seismic performance of storage steel tanks during the May 2012 Emilia, Italy, earthquakes, J. Perform. Constr. Facil. 29 (5) (2015)https://doi.org/10.1061/(ASCE)CF.1943-5509.0000628 04014137.
[5] K.B. McGrattan, H.R. Baum, A. Hamins, Thermal Radiation from Large Pool Fires, 6546, NIST Technology Administration U.S. Department of Commerce, NISTIR, November 2000.
[6] K.A. Mansour, Fires in Large Atmospheric Storage Tanks and their Effect on Adjacent Tanks(Doctoral Dissertation) Loughborough University, 2012.
[7] W. He Wang, Z. Sheng Xu, B. Jiang Sun, Numerical simulation of fire thermal radiation field for large crude oil tank exposed to pool fire, Process. Eng. 52 (2013) 395–400.
[8] M. Munoz, E. Planas, F. Ferrero, J. Casal, Predicting the emissive power of hydrocarbon pool fires, J. Hazard. Mater. 144 (2007) 725–729.
[9] A. Sengupta, A.K. Gupta, I.M. Mishra, Engineering layout of fuel tanks in a tank farm, J. Loss Prev. Process Ind. 24 (2011) 568–574.
[10] G. Landucci, G. Gubinellia, G. Antonioni, V. Cozzani, The assessment of the damage probability of storage tanks in domino events triggered by fire, Accid. Anal. Prev. 41 (6) (2009) 1206–1215.
[11] F. da Silva Santos, A. Landesmann, Thermal performance based analysis of minimum safe distances between fuel storage tanks exposed to fire, Fire Saf. J. 69 (2014) 57–68.
[12] M.R. Eslami, R. Shahsiah, Thermal buckling of imperfect cylindrical shells, J. Therm. Stresses 24 (2001) 71–89.
[13] M.R. Eslami, A.R. Ziaii, A. Ghorbanpour, Thermoelastic buckling of thin cylindrical shells based on improved Donnell equations, J. Therm. Stresses 19 (1996) 299–316.
[14] E.A. Thornton, Thermal buckling of plates and shells, Appl. Mech. Rev. 46 (10) (1993) 485–506.
[15] N.J. Hoff, C. Chao, W.A. Madsen, Buckling of a thin-walled circular cylindrical shell heated along an axial strip, J. Appl. Mech. 31 (2) (1964) 253–258.
[16] B. Ross, N.J. Hoff, W.H. Horton, The buckling behaviour of uniformly heated thin circular cylindrical shells, J, Exp. Mech. 6 (11) (1966) 529–537.
[17] B. Ross, J. Mayers, A. Jaworski, Buckling of thin cylindrical shells heated along an axial strip, J, Exp. Mech. 5 (8) (1965) 247–256.
[18] L.A. Godoy, Buckling of vertical oil storage steel tanks: review of static buckling studies, Thin-Walled Struct. 103 (2016) 1–21.
[19] Y. Liu, Thermal Buckling of Metal Oil Tanks Subject to an Adjacent Fire(Doctoral Dissertation) The University of Edinburg, 2011.
[20] L.A. Godoy, J.C. Batista-Abreu, Buckling of fixed roof above ground oil storage tanks under heat induced by an external fire, Thin-Walled Struct. 52 (2012) 90–101.
[21] J.C. Batista-Abreu, L.A. Godoy, Thermal buckling behaviour of open cylindrical oil storage tanks under fire, J. ASCE. Perf. Constr. Facil. 27 (1) (2013) 1–9.
[22] C.A. Burgos, J.C. Batista-Abreu, H.D. Calabró, R.C. Jaca, L.A. Godoy, Buckling estimates for oil storage tanks: effect of simplified modelling of the roof and wind girder, Thin-Walled Struct. 91 (2015) 29–37.
[23] P.M. Baiz, M.H. Aliabadi, Buckling analysis of shear deformable shallow shells by the boundary element method, Eng. Anal. Bound. Elem. 31 (4) (2007) 361–372.
[24] H.T. Chien, H.X. Nguyen, N.T. Nguyen, T.H. Le, T.T. Nguyen, T. Rabczuk, Static, free vibration and buckling analysis of laminated composite Reissner-Mindlin plates using NURBS-based isogeometric approach, Int. J. Numer. Methods Eng. 91 (2012) 571–603.
[25] H.T. Chien, H.X. Nguyen, N.T. Nguyen, T.H. Le, T.T. Nguyen, T. Rabczuk, Isogeometric analysis for large deformation thin-shells using RHT-splines for multiple-patch coupling, Comput. Methods Appl. Mech. Eng. 316 (2017) 1157–1178.
[26] MSC Software Corporation, MSC Marc, Theory and User Information, Version 2014, vol. A, 2014.
[27] R. Nascimbene, Towards non–standard numerical modelling of thin-Shell structures: geometrically linear formulation, Int. J. Comput. Methods Eng. Sci. Mech. 15 (2) (2014) 126–141.
[28] T. Belytschko, B.L. Wong, H.-Y. Chiang, Advances in one-point quadrature shell elements, Comput. Methods Appl. Mech. Eng. 96 (1) (1992) 93–107.
[29] R. Nascimbene, P. Venini, A new locking-free equilibrium mixed element for plane elasticity with continuous displacement interpolation, Comput. Methods Appl. Mech. Eng. 191 (17–18) (2002) 1843–1860.
[30] T. Belytschko, H. Stolarski, W.K. Liu, N. Carpenter, J.S.-J. Ong, Stress projection for membrane and shear locking in shell finite elements, Comput. Methods Appl. Mech. Eng. 51 (1985) 221–258.

[31] T.J.R. Hughes, T.E. Tezduyar, Finite elements based upon Mindlin plate theory with particular reference to the four-node bilinear isoparametric element, J. Appl. Mech. 48 (3) (1981) 587–596.
[32] T.J.R. Hughes, The Finite Element Method: Linear Static and Dynamic Finite Element Analysis, Prentice-Hall Englewoods Cliffs, New Jersey, 1987.
[33] K.J. Bathe, E.N. Dvorkin, A four-node plate bending element based on Mindlin/Reissner theory and a mixed interpolation, Int. J. Numer. Methods Eng. 21 (1985) 367–383.
[34] European Committee For Standardization, EN 1993-1-2, eurocode 3: design of steel structures–Part 1–2, General Rules–Structural Fire Design, 2003.
[35] T. Kobayashi, Y. Mihara, F. Fujii, Artificial damping method for local instability problems in shells, in: Gorski Pietraszkiewicz (Ed.), Shell Structures: Theory and Applications, Taylor and Francis Group, London, 2014.
[36] C. Yu, B.W. Schafer, Simulation of cold formed steel beams in local and distortional buckling with applications to the direct strength method, J. Constr. St. Res. 63 (2007) 581–590.
[37] J. Singer, J. Arbocz, T. Weller, Buckling experiments, experimental methods in buckling of thin-walled structures, Shells, Built-up Structures, Composites and Additional Topics, vol. 2, John Wiley and Sons, 2002.